Available online at www.sciencedirect.com
ScienceDirect
Journal of Membrane Science 305 (2007) 353–363
journal of MEMBRANE SCIENCE
www.elsevier.com/locate/memsci

Synthesis and properties of fluorine-containing polybenzimidazole/silica nanocomposite membranes for proton exchange membrane fuel cells

Shih-Wei Chuang, Steve Lien-Chung Hsu *, Yen-Hsin Liu

Department of Materials Science and Engineering, Frontier Material and Micro/Nano Science and Technology Center, National Cheng-Kung University, 1 Ta-Hsueh Road, Tainan 70101, Taiwan, ROC

Received 27 June 2007; received in revised form 11 August 2007; accepted 16 August 2007
Available online 19 August 2007

Abstract

Novel polybenzimidazole (PBI)/silica nanocomposite membranes were prepared via sol–gel process from an organosoluble, fluorine-containing PBI copolymer with a silica precursor, tetraethoxysilane (TEOS), and a bonding agent. The introduction of the bonding agent results in the reinforced interfacial interaction between PBI chains and silica nanoparticles. Transmission electron microscopy (TEM) analyses showed that the silica particles were well dispersed in the PBI matrix on a nanometer scale. The thermooxidative stability of the PBI membranes increased slightly with the increase of silica content. The coefficients of the thermal expansion (CTEs) of the nanocomposite membranes decreased slightly with increasing amounts of silica. The mechanical properties and the methanol barrier ability of the PBI films were improved by the addition of silica. The modulus of the PBI/10 wt.% silica nanocomposite membranes had a 37% increase compared to the pure PBI films, and the methanol permeability decreased by 58% with respect to the pure PBI membranes. The conductivities of the acid-doped PBI/silica nanocomposites were slightly lower than the acid-doped pure PBI.

Keywords: Polybenzimidazole; Nanocomposite; Fuel cell; Silica; Sol–gel process

1. Introduction

Proton exchange membranes (PEMs) have received a lot of attention in recent years, because they are the most important part in proton exchange membrane fuel cells (PEMFCs). PEMs function as conductive proton mediums, as well as barriers to avoid direct contact between the fuel and oxidant. In order to alleviate the effect of CO poisoning in electrodes and to improve the power density of the fuel cells, the operating temperature has been proposed to be maintained above 100 °C. The perfluorosulfonic acid polymer membranes, such as Nafion®, are typically used as the electrolytes in PEMFCs, because of their outstanding chemical stability and high proton conductivity. However, the Nafion® membranes have two major drawbacks: (i) loss of proton conductivity at temperatures above 100 °C due to dehydration phenomena; (ii) high methanol permeation, which causes loss of fuel and decreases cathode performance in PEMFCs [1–7]. Polybenzimidazole (PBI) is a very promising material for high-temperature (>100 °C) fuel cell applications, because of its high thermal stability and good mechanical properties. In addition, PBI doped with strong acids has stable proton conductivity at temperatures higher than 100 °C [8–16].

The preparation of hybrid organic–inorganic composites has been developed and studied during the last decade, because hybrids show controllable chemical and physical properties by combining the effects of organic polymers and inorganic compounds [17–23]. Several studies have showed that the presence of silica particles in the organic polymer matrix can reduce the methanol permeability of the hybrids due to the dispersed silica particles acting as methanol barriers [24–26]. Therefore, the polymer/silica hybrid membranes have the potential for use as PEMs.

In this study, we have prepared novel PBI/silica hybrid membranes using a silica precursor, tetraethoxysilane (TEOS), via a sol–gel process in a PBI solution, followed by solution casting. The PBI used in this research is an amorphous, organosoluble fluorine-containing PBI. Compared to the most commonly PBI used in PEMFCs, poly[2,2′-(*m*-phenylene)-5,5′-bibenzimidazole], which is difficult to dissolve in common organic solvents due to its very rigid molecular structure, the

* Corresponding author. Tel.: +886 6 2757575x62904; fax: +886 6 2346290.
E-mail address: lchsu@mail.ncku.edu.tw (S.L.-C. Hsu).

0376-7388/$ – see front matter © 2007 Elsevier B.V. All rights reserved.
doi:10.1016/j.memsci.2007.08.033

fluorine-containing PBI is soluble in several organic solvents. It could be used to prepare PBI/silica hybrid membranes through the sol–gel process. However, the great difference in the properties of polymer and silica materials may cause phase separation. In order to avoid phase separation, some papers have reported that a bonding agent can be added to bond the organic moiety and the inorganic phase [27–29]. To achieve this objective, a fluorine-containing PBI copolymer containing hydroxyl groups was synthesized in this research to provide the bonding sites for the bonding agent. The fluorine-containing PBI copolymer had good compatibility with the inorganic silica phase. Here, we report the mechanical properties, thermal properties and methanol permeability of the PBI/silica hybrid membranes. The proton conductivities of these hybrid films doped with phosphoric acid were also examined.

2. Experimental

2.1. Materials

2,2-Bis(4-carboxyphenyl)hexafluoropropane was purchased from TCI and purified by recrystallization from glacial acetic acid. 3,3′-Diaminobenzidine, triethylamine, and dimethylacetamide (DMAc) were obtained from Aldrich. 5-Hydroxyisophthalic acid, tetraethoxysilane (TEOS) and diethylamine were obtained from Acros. 3,3′-Diaminobenzidine and 5-hydroxyisophthalic acid were used as received, and DMAc was purified by distillation over calcium hydride. Reagent-grade poly(phosphoric acid) (PPA), phosphoric acid and (3-isocyanatopropyl)triethoxysilane were obtained from Fluka and used as supplied. Other chemicals and solvents were used as received.

2.2. Polymer synthesis

The reaction is shown in Scheme 1. A typical preparation of the PBI30OH ($x = 0.3n$, $y = 0.7n$) proceeds as follows: In a 250-mL, three-necked, round-bottom flask equipped with a mechanical stirrer and a condenser, 0.2679 g (1.25 mmol) of 3,3′-diaminobenzidine was dissolved in 12.9067 g of PPA. The solution was stirred until it became homogeneous. To the solution, 0.3432 g (0.875 mmol) of 2,2-bis(4-carboxyphenyl)hexafluoropropane and 0.0683 g (0.375 mmol) of 5-hydroxyisophthalic acid were added, and the mixture was reacted at 200 °C for 24 h. The reaction mixture was cooled to 70 °C. The PPA with P_2O_5 content at 84.5% was diluted with 85% phosphoric acid and water to reduce the P_2O_5 content to approximate 67%. The homogeneous solution was stirred overnight to hydrolyze the phosphate ester. The resulting solution was added dropwise to 1 L of deionized water while being stirred. The precipitated polymer was collected by filtration and washed with deionized water several times. The polymer was dried in vacuum at 100 °C for 24 h. The synthesis of PBI10OH ($x = 0.1n$, $y = 0.9n$) followed the same procedure.

2.3. Preparation of PBI/silica nanocomposite membranes

A representative 10 wt.% silica loading PBI30OH/silica nanocomposite was prepared as follows: the PBI30OH powder (1.053 g) was dissolved in 35.1 g of DMAc to make a 3 wt.% solution. 0.175 g of (3-isocyanatopropyl)triethoxysilane was added to the PBI30OH solution as a bonding agent (molar ratio of hydroxyl group/bonging agent = 1). A catalytic amount of triethylamine was also added, and the mixture was stirred for 36 h at room temperature with a nitrogen inlet. Then, 0.2929 g of TEOS and 0.0988 g of deionized water were added to the viscous solution (molar ratio of H_2O/TEOS = 4). A catalytic amount of diethylamine was also added, and the homogeneous solution was further stirred for 24 h at room temperature. The solution was cast onto a glass plate with a doctor's knife and dried in a vacuum oven at room temperature for 24 h. It was further dried in vacuum at 110 °C for 2 days to complete the hydrolysis and condensation of silica. The reaction is shown in Scheme 2. The thickness of the PBI/silica nanocomposite membranes was approximately 40 μm. The membranes were doped by immersion in aqueous phosphoric acid (11 M) for different times. The amount of phosphoric acid in each film was dependent on the immersion time, and calculated by weight analysis. The phosphoric acid-doped PBIs were coded as PBI–$x$$H_3PO_4$, with x as the number of moles of acid per repeat unit of PBI.

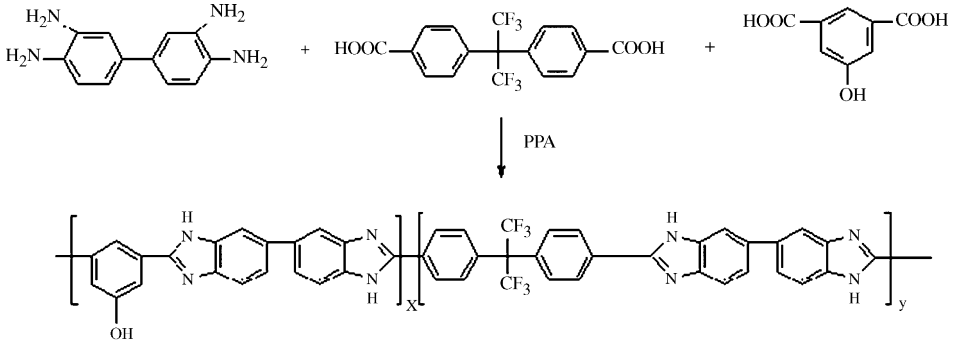

PBI10OH--- x=0.1n, y=0.9n

PBI30OH--- x=0.3n, y=0.7n

Scheme 1. Synthesis of fluorine-containing PBI copolymer.

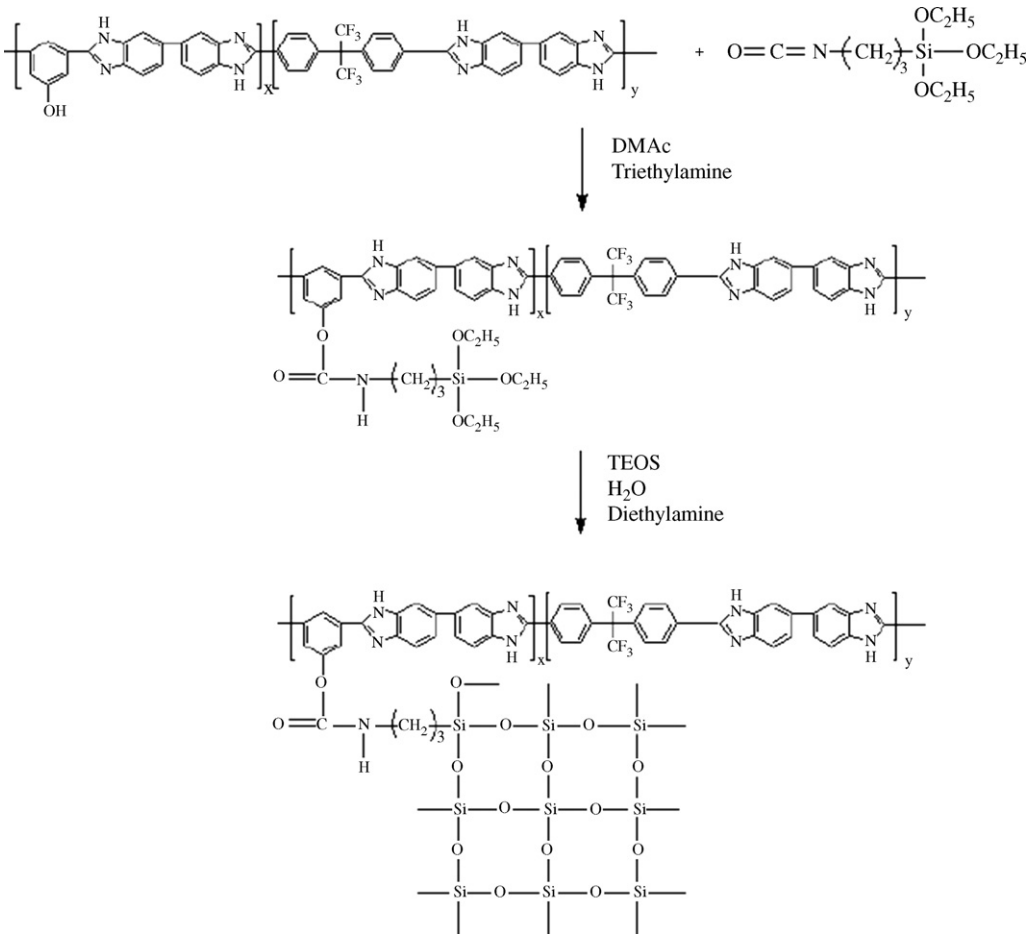

Scheme 2. Synthesis of PBI/silica hybrid material.

2.4. Characterization

The IR spectra were recorded on a Jasco 460 FTIR spectrometer. The ^{1}H NMR spectrum was recorded on a Bruker AV-500 spectrometer. The inherent viscosity was measured with a Cannon-Ubbelohde no. 100 viscometer at a concentration of 0.5 g/dL in DMAc at 30 °C. The wide angle X-ray diffraction (WAXD) experiment was conducted on a Rigaku (Tokyo, Japan) D/MAX-IIIV X-ray diffractometer with Cu Kα radiation. The samples for transmission electron micrograph (TEM) study were prepared by placing the PBI/silica nanocomposite films in an epoxy resin that was cured at 70 °C overnight. The cured epoxies containing PBI/silica nanocomposite films were microtomed with a diamond knife into 50-nm-thick slices. Next, they were placed on a 200-mesh copper grid, and examined with a Hitachi HF-2000 TEM (equipped with an energy dispersive X-ray (EDX) spectrometer) using an acceleration voltage of 200 kV. The thermoxaditive stability was analyzed with a TA Instrument 2050 Thermogravimetric analyzer (TGA) at a heating rate of 10 °C/min under air. The in-plane coefficients of thermal expansion (CTEs) and dynamic thermal mechanical analysis (DTMA) of PBI/silica nanocomposite membranes were determined using a TA Instrument Thermal Mechanical Analyzer (TMA) Q400EM. The CTEs were measured with an extension probe under 0.05 N tension force on the films in the temperature range of 100–250 °C at a heating rate of 5 °C/min under nitrogen. The DTMA was measured at a heating rate of 5 °C/min in nitrogen under a modulated force of 0.05 N at a frequency of 1 Hz. Tensile properties were determined from stress–strain curves obtained with a Shimadzu AG-SI universal testing machine at a strain rate of 5 mm/min at room temperature. The film specimens were 30 mm long, 4.5 mm wide, and 40 μm thick. The conductivity measurement was performed with an Autolab PGSTST 30 impedance analyzer in the frequency range of 100–10^5 Hz with an amplitude of 10 mV. The measurement cell is shown in Fig. 1. The measurements were taken at 160 °C

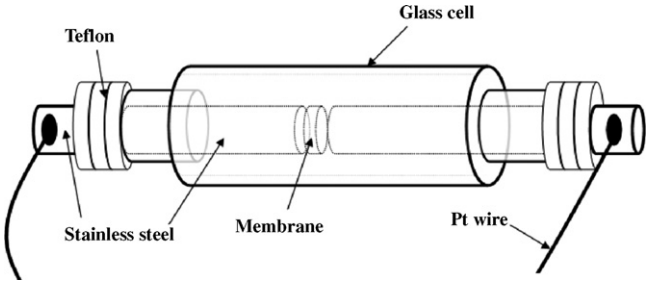

Fig. 1. Schematic diagram of proton conductivity measurement cell.

under anhydrous condition. The conductivity (σ) was calculated as follows:

$$\sigma = \frac{1}{R}\frac{L}{A}$$

where R, L, and A are the measured resistance, thickness, and cross-sectional area of the membrane, respectively. The methanol permeability was measured with a two-compartment glass cell. One source cell ($V_A = 100$ mL) was filled with a 6 wt.% methanol aqueous solution. The other receiving cell ($V_B = 100$ mL) was filled with deionized water. The membrane was clamped between the two compartments. The concentration of methanol in the receiving cell was measured versus time by gas chromatography with a Shimadzu QP2010. The methanol concentration in the receiving cell is given by

$$C_B(t) = \frac{A}{V_B}\frac{P}{L}C_A(t - t_0)$$

where C_B and C_A are the methanol concentration in the receiving cell and the source cell, respectively, V_B the volume of the receiving cell, and P is the methanol permeability. t_0, also termed the time lag, is related to the methanol diffusion coefficient (D) as follows: $t_0 = L^2/6D$ [30,31].

3. Results and discussion

3.1. Synthesis and characterization of PBI and PBI/silica nanocomposites

Fluorine-containing PBI was synthesized from 3,3′-diaminobenzidine, 2,2-bis(4-carboxyphenyl)hexafluoropropane, and 5-hydroxyisophthalic acid. The purpose of using the 2,2-bis(4-carboxyphenyl)hexafluoropropane monomer was to modify the properties of PBI, such as the flexibility, solubility and processability. The 5-hydroxyisophthalic acid monomer was introduced to provide the bonding sites to the bonding agents. However, according to the study of Chen et al. [32], phosphate ester could be formed between the hydroxyl groups and PPA. In our research, we eliminated the phosphate ester by hydrolysis during the work-up step by the addition of phosphoric acid and water. The inherent viscosities of PBI10OH and PBI30OH were 1.8 and 1.4 dL/g, respectively, which were measured in DMAc at a concentration of 0.5 g/dL at 30 °C, indicating that the two PBI copolymers had high molecular weights. The formation of the PBI copolymers was confirmed by the IR and ^{1}H NMR spectra, as shown in Figs. 2 and 3. The PBI10OH and PBI30OH exhibited characteristic IR absorption bands at 3400–3100 cm^{-1} due to the N–H and O–H groups, and an absorption band at 1625 cm^{-1} due to the C=N absorption. The ^{1}H NMR spectra of PBI copolymers were measured in deuterated dimethylsulfone. The imidazole proton peaks of PBI10OH and PBI30OH were observed at 13.1–13.3 ppm, and the hydroxyl protons were observed at 10.1–10.3 ppm.

Table 1 summarizes the qualitative solubility of the PBI copolymers. PBI10OH and PBI30OH were soluble in several organic solvents. This could be due to the introduction of bulky hexafluoropropylidene bridging groups in the polymer backbone, which reduces the intermolecular forces between the polymer chains. The PBI copolymer membranes were easily fabricated from the PBI copolymer solutions in DMAc via solution casting.

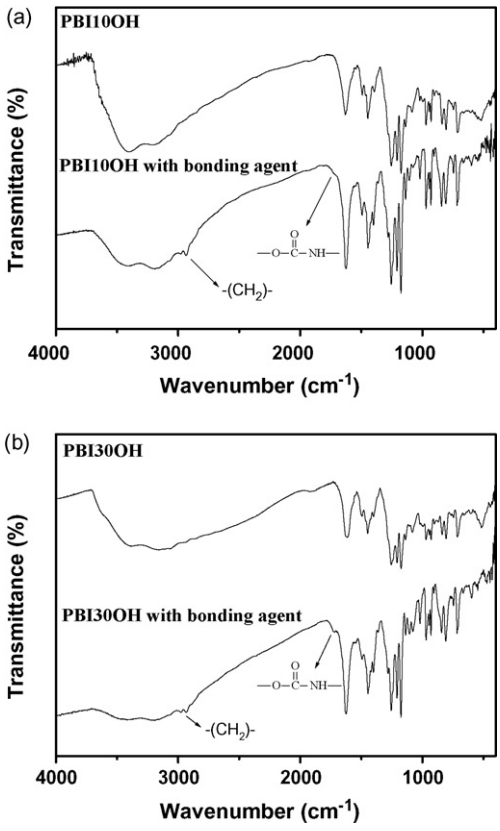

Fig. 2. IR spectra of PBI10OH and that with bonding agent (a) and PBI30OH and that with bonding agent (b).

To study the morphology of the PBI copolymers, the films prepared from the copolymers were examined with WAXD measurements. Fig. 4 shows the WAXD patterns of PBI10OH and PBI30OH. They do not show any obvious diffraction peak. This indicates that the two PBI copolymers are amorphous due to the bulky –$(CF_3)_2$ groups in the backbones. The absence of crystal-

Table 1
Solubility of the PBI copolymers

Solvent[a]	Solubility[b]	
	PBI10OH	PBI30OH
NMP	+	+
DMAc	+	+
DMSO	+	+
DMF	+	+
MSA	+	+
Methanol	−	−
THF	−	−
Chloroform	−	−
Acetone	−	−

[a] NMP, *N*-methyl-2-pyrrolidone; DMAc, dimethylacetamide; DMSO, dimethylsulfone; DMF, dimethylformamide; MSA, methanesulfonic acid; THF, tetrahydrofuran.
[b] (+) soluble; (−) insoluble.

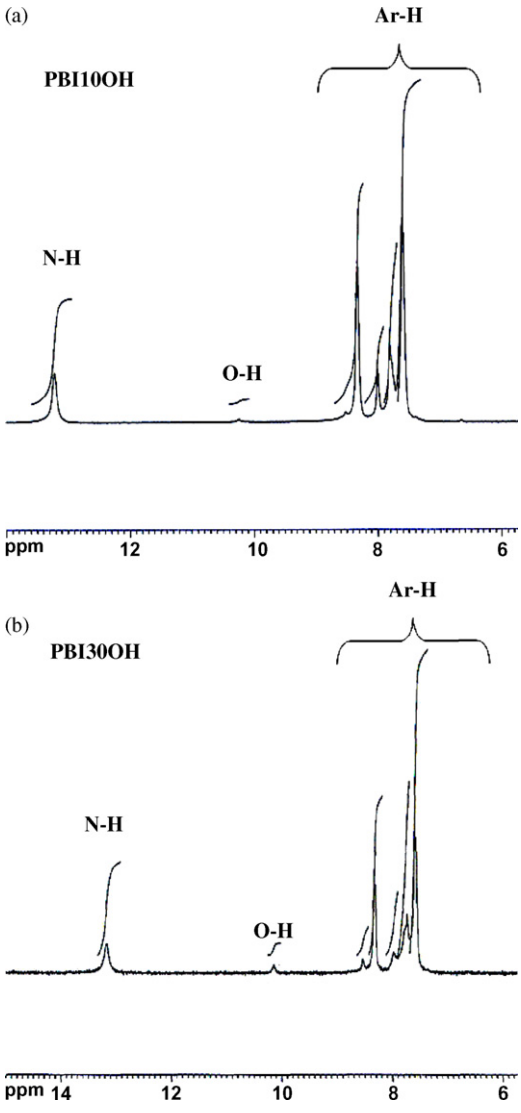

Fig. 3. ^{1}H NMR spectra of PBI10OH (a) and PBI30OH (b).

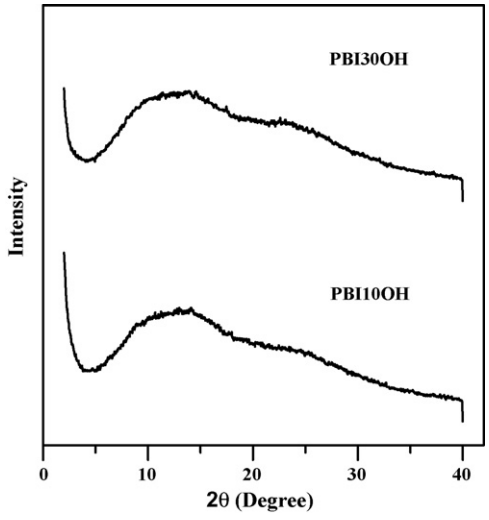

Fig. 4. WAXD patterns of PBI10OH and PBI30OH.

lization in the PBI copolymers was beneficial for dissolution in organic solvents and for proton conductivity [33,34].

Some papers reported that the condensation between the hydroxyl group of the polymer and silanol generated by hydrolysis of TEOS was difficult due to the poor reactivity of aromatic hydroxyl group with silanol [35,36]. For this reason, bonging agents were introduced to form covalent bonds between the PBI copolymers and silica. The formation of bonds between the PBI copolymers and bonging agents was indicated by the absence of the –N=C=O absorption band of the isocyanato group on the bonding agent (2270 cm^{-1}), the presence of weak C=O stretching band of the urethane group (1725 cm^{-1}) and the –(CH_2)-absorption band of the bonding agent (3000–2900 cm^{-1}), as shown in Fig. 2.

3.2. Morphology of PBI/silica nanocomposite membranes

TEM micrographs of PBI10OH/10 and 15 wt.% silica nanocomposites and PBI30OH/10 and 15 wt.% silica nanocomposites are shown in Figs. 5 and 6. The grey part is the polymer matrix, the dark dots are the silica particles that were confirmed by using EDX spectrum shown in Fig. 7. The average silica particle sizes of PBI10OH/10 and 15 wt.% silica nanocomposites are 24 and 38 nm, respectively. Well-dispersed silica particles are observed in the PBI10OH/10 wt.% silica nanocomposites, and a couple of agglomerated nanosized particles are seen in the PBI10OH/15 wt.% silica nanocomposites. This result shows that the content of the silica is too much when 15 wt.% of silica was added to PBI10OH. The average silica particle sizes of PBI30OH/10 and 15 wt.% silica nanocomposites are 17 and 28 nm, respectively. The silica particle distributions of PBI30OH/silica nanocomposites show a similar trend as that of PBI10OH/silica nanocomposites. However, the average silica particle sizes of PBI30OH/10 and 15 wt.% silica nanocomposites are smaller than that of PBI10OH/10 and 15 wt.% silica nanocomposites. This phenomenon may be caused by more hydroxyl groups being presented in PBI30OH as bonding sites to the inorganic silica.

3.3. Thermal properties of PBI/silica nanocomposite membranes

The thermooxidative stability of PBI10OH/silica nanocomposites and PBI30OH/silica nanocomposites were studied using TGA in air. The results are shown in Fig. 8. The two pure PBI copolymers displayed high thermooxidative stability. The 5% weight loss temperatures of PBI10OH/silica nanocomposites and PBI30OH/silica nanocomposites are listed in Table 2. The decomposition temperatures of the nanocomposites increased slightly with increasing amounts of silica. The increase in thermal stability could be attributed to the high thermal stability of silica. The 5% weight loss temperatures of PBI10OH/15 wt.% silica nanocomposites and PBI30OH/15 wt.% silica nanocomposites increased 6 and 13 °C relative to the pure PBI10OH and PBI30OH copolymers, respectively. The increase in decomposition temperature of PBI30OH/15 wt.% silica nanocomposites was higher than that of PBI10OH/15 wt.% silica nanocom-

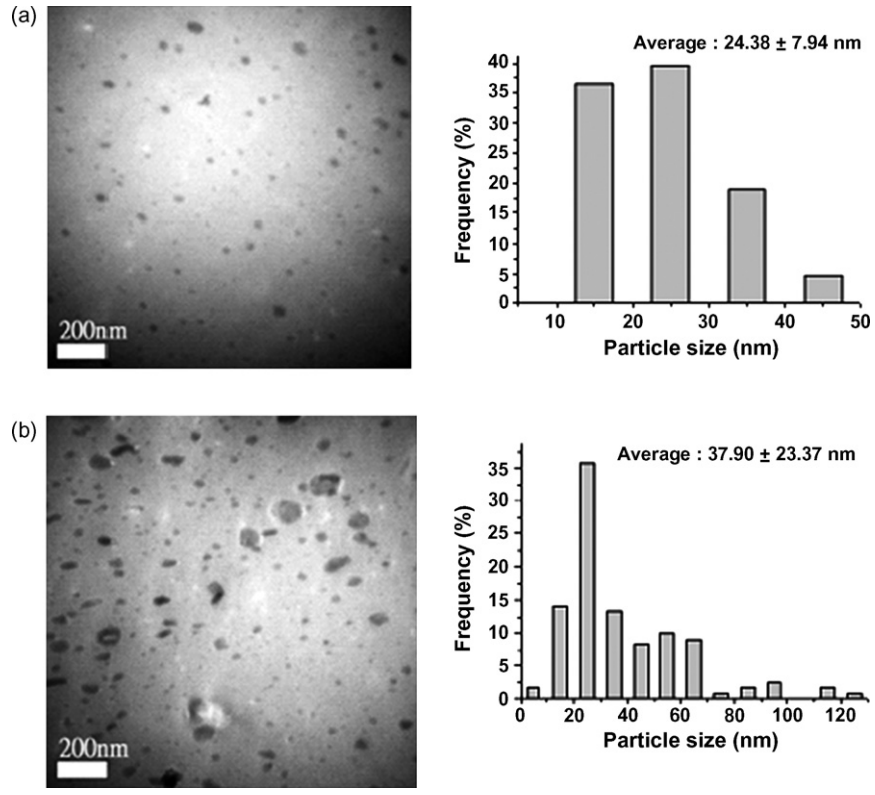

Fig. 5. TEM micrographs and particle size distributions of PBI10OH/10 wt.% silica nanocomposite (a) and PBI10OH/15 wt.% silica nanocomposite (b).

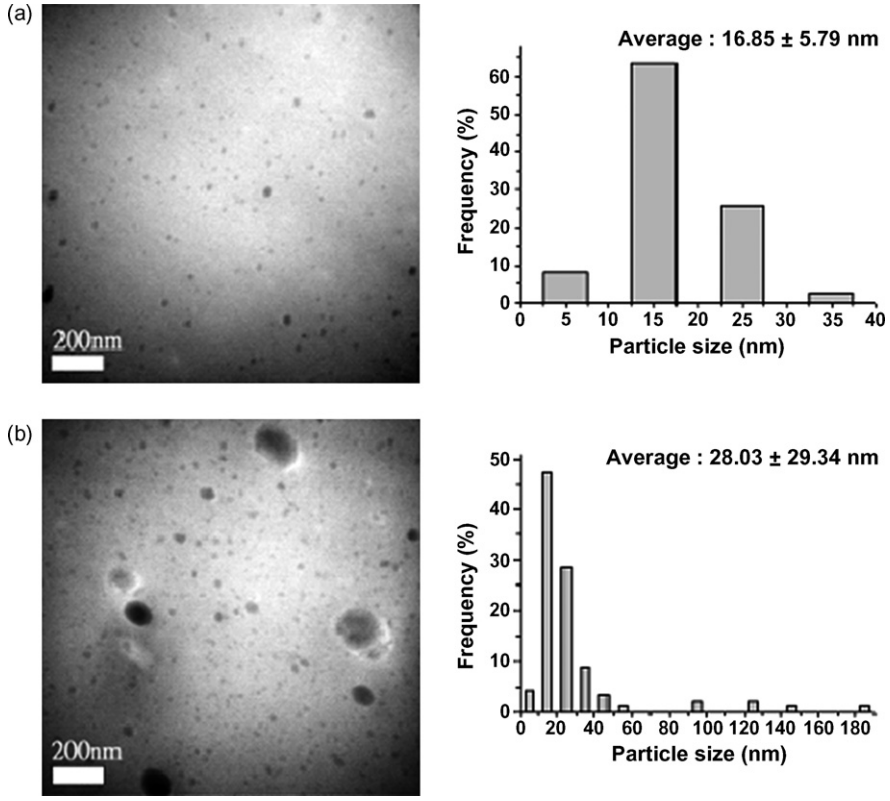

Fig. 6. TEM micrographs and particle size distributions of PBI30OH/10 wt.% silica nanocomposite (a) and PBI30OH/15 wt.% silica nanocomposite (b).

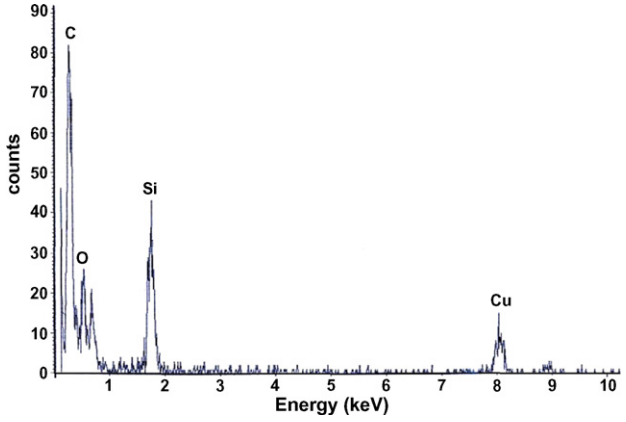

Fig. 7. EDX spectrum of PBI30OH/15 wt.% silica nanocomposite.

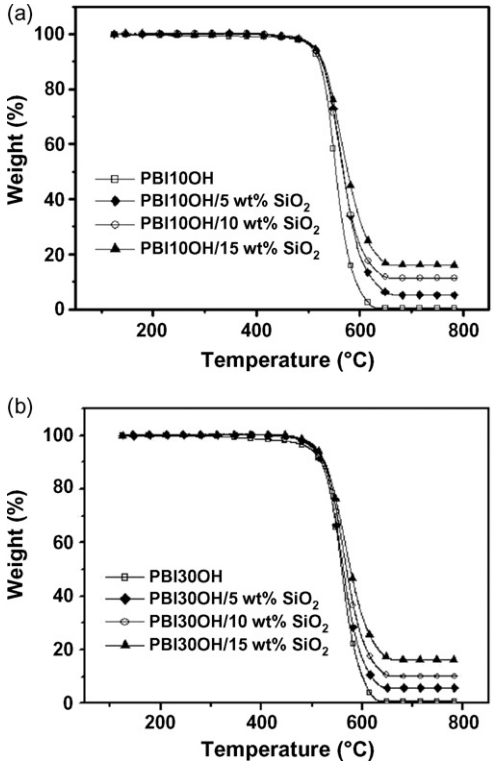

Fig. 8. TGA thermograms of PBI10OH/silica nanocomposites (a) and PBI30OH/silica nanocomposites (b) in air.

Table 2
Thermal properties of the PBI copolymers

	CTEs[a] (μm/m °C)	T_g[b] (°C)	T_5[c] (°C)
PBI10OH	25.4	334	508
PBI10OH/5 wt.% SiO_2	24.4	337	511
PBI10OH/10 wt.% SiO_2	23.7	338	512
PBI10OH/15 wt.% SiO_2	21.3	337	514
PBI30OH	21.4	321	496
PBI30OH/5 wt.% SiO_2	19.8	322	503
PBI30OH/10 wt.% SiO_2	17.6	325	507
PBI30OH/15 wt.% SiO_2	16.3	325	509

[a] Coefficient of thermal expansion, measured by TMA in the temperature range of 100–250 °C.
[b] Glass transition temperature, identified by tan δ_{max}.
[c] Temperature of 5% weight loss, as determined by TGA in air.

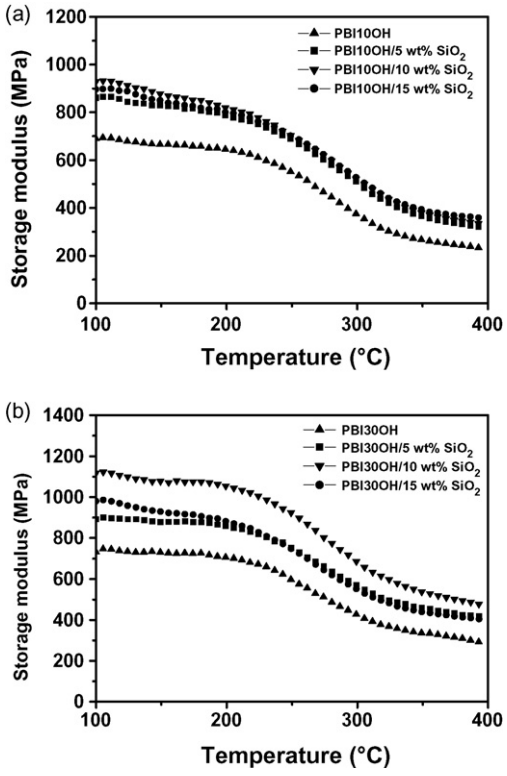

Fig. 9. Storage moduli of PBI10OH/silica nanocomposites (a) and PBI30OH/silica nanocomposites (b).

posites, because of more hydroxyl groups being presented in the PBI30OH as bonding sites to the silica phase. The residual weight percentages of PBI10OH/silica nanocomposites and PBI30OH/silica nanocomposites above 700 °C were approximately proportional to theoretical silica loadings. It indicated that the conversion of silica was complete via the sol–gel process.

The in-plane CTEs of PBI10OH/silica nanocomposites and PBI30OH/silica nanocomposites are listed in Table 2. It was found that the CTEs of PBI10OH/silica nanocomposites and PBI30OH/silica nanocomposites slightly decreased with increasing amounts of silica. This indicated that silica could reduce the thermal expansion of the PBI copolymers.

The storage moduli of PBI10OH/silica nanocomposites and PBI30OH/silica nanocomposites are presented in Fig. 9. The storage moduli of PBI10OH/silica nanocomposites and PBI30OH/silica nanocomposites increased with increasing amounts of silica up to a silica content of 10 wt.%. The tan δ of PBI10OH/silica nanocomposites and PBI30OH/silica nanocomposites are shown in Fig. 10. The tan δ_{max} was identified as the glass transition temperature (T_g). The T_gs of PBI10OH/silica nanocomposites and PBI30OH/silica nanocomposites are listed in Table 2, which could not be found in differential scanning calorimeter (DSC)measurement. The T_gs of PBI10OH/silica nanocomposites and PBI30OH/silica nanocomposites slightly increased with increasing amounts of silica. The increase in storage moduli, and tan δ of the nanocomposites might be caused by the interaction between the inorganic silica and the organic PBI copolymers [37–39].

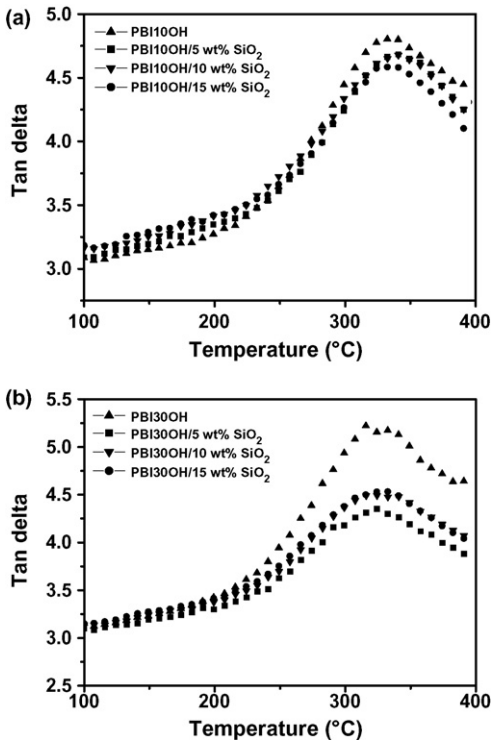

Fig. 10. tan δ of PBI10OH/silica nanocomposites (a) and PBI30OH/silica nanocomposites (b).

3.4. Mechanical properties of PBI/silica nanocomposite membranes

Tables 3 and 4 summarize the tensile properties of PBI10OH/silica nanocomposites and PBI30OH/silica nanocomposites. The tensile moduli and strength of PBI10OH/silica nanocomposites and PBI30OH/silica nanocomposites increased with the increase of silica content up to a silica content of 10 wt.%. These reinforcing effects might result from the interfacial interaction between PBI chains and silica particles. The moduli of PBI10OH/10 wt.% silica nanocomposites and PBI30OH/10 wt.% silica nanocomposites increased 17 and 37% compared to the pure PBI10OH and PBI30OH copolymers, respectively. The larger increase in modulus of PBI30OH/10 wt.% silica nanocomposites could be attributed to more hydroxyl groups being presented in the PBI30OH as bonding sites to the silica phase. The modulus of the PBI30OH/10 wt.% silica nanocomposites without bonding agents increased only by 11% compared to the pure PBI30OH due to the lack of strong interfacial interactions between the PBI chains and the silica particles. Both the tensile moduli and strength of PBI10OH/silica nanocomposites and PBI30OH/silica nanocomposites slightly decreased when the silica content reached 15 wt.%. The phenomenon might be caused by a few agglomerated nanosized silica particles in the polymer matrix.

Tables 3 and 4 also summarize the tensile properties of PBI10OH/silica nanocomposites and PBI30OH/silica nanocomposites doped with phosphoric acid. It was found that the tensile moduli and strength of the nanocomposites decreased when they were doped with phosphoric acid. This could be due

Table 3
Mechanical properties of PBI10OH/silica nanocomposite membranes and phosphoric acid-doped PBI10OH/silica nanocomposite membranes

	Modulus (GPa)	Stress (MPa)	Elongation (%)
PBI10OH	1.17 ± 0.13	80.1 ± 5.4	13.7 ± 2.5
PBI10OH/5 wt.% SiO_2	1.29 ± 0.07	84.2 ± 5.0	12.1 ± 0.7
PBI10OH/10 wt.% SiO_2	1.37 ± 0.05	99.0 ± 6.6	11.5 ± 0.6
PBI10OH/15 wt.% SiO_2	1.30 ± 0.04	90.3 ± 5.8	11.4 ± 1.0
PBI10OH–3.0H_3PO_4	0.55 ± 0.12	42.0 ± 6.8	32 ± 1.3
PBI10OH/5 wt.% SiO_2–3.0H_3PO_4	0.70 ± 0.04	48.3 ± 4.8	26.2 ± 1.8
PBI10OH/10 wt.% SiO_2–3.0H_3PO_4	0.84 ± 0.10	49.9 ± 3.7	25.7 ± 3.1
PBI10OH/15 wt.% SiO_2–3.0H_3PO_4	0.73 ± 0.02	48.9 ± 3.4	26.9 ± 3.7

Table 4
Mechanical properties of PBI30OH/silica nanocomposite membranes and phosphoric acid-doped PBI30OH/silica nanocomposite membranes

	Modulus (GPa)	Stress (MPa)	Elongation (%)
PBI30OH	1.62 ± 0.12	89.8 ± 4.8	11.7 ± 1.5
PBI30OH/5 wt.% SiO_2	1.81 ± 0.09	102.7 ± 4.8	11.0 ± 0.7
PBI30OH/10 wt.% SiO_2 (without bonding agent)	1.80 ± 0.13	84.4 ± 5.9	9.5 ± 1.7
PBI30OH/10 wt.% SiO_2	2.22 ± 0.07	113.8 ± 5.0	10.8 ± 1.0
PBI30OH/15 wt.% SiO_2	2.15 ± 0.06	92.2 ± 5.9	8.3 ± 2.1
PBI30OH–3.0H_3PO_4	0.83 ± 0.06	41.4 ± 0.6	34.9 ± 4.5
PBI30OH/5 wt.% SiO_2–3.0H_3PO_4	0.88 ± 0.04	41.2 ± 1.4	20.1 ± 4.7
PBI30OH/10 wt.% SiO_2–3.0H_3PO_4	1.15 ± 0.01	57.5 ± 1.3	10.9 ± 3.6
PBI30OH/15 wt.% SiO_2–3.0H_3PO_4	1.11 ± 0.04	51.9 ± 2.7	14.8 ± 3.3

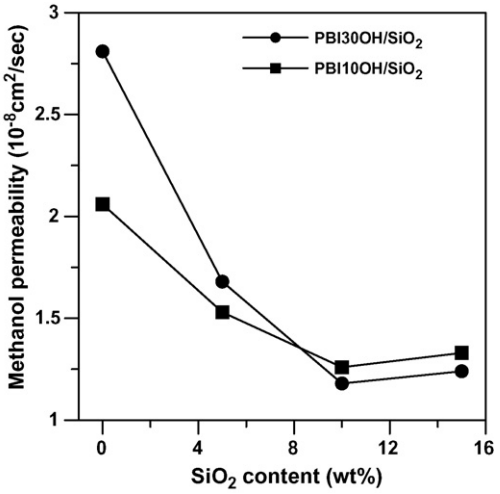

Fig. 11. Methanol permeability of PBI10OH/silica nanocomposites and PBI30OH/silica nanocomposites in 6 wt.% methanol aqueous solution at room temperature.

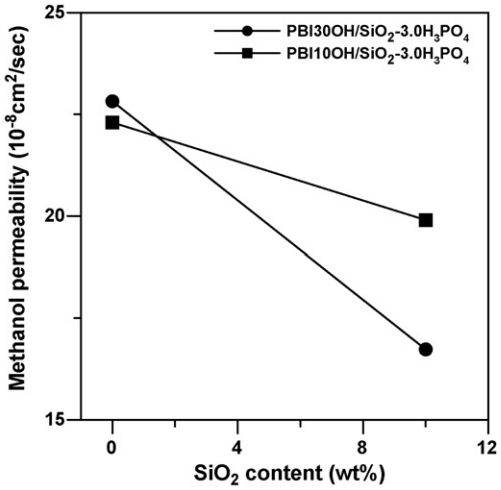

Fig. 12. Methanol permeability of PBI10OH/silica nanocomposites and PBI30OH/silica nanocomposites doped with phosphoric acid (in 6 wt.% methanol aqueous solution at room temperature).

to the plasticizing effect from the phosphoric acid. However, the PBI30OH/10 wt.% silica nanocomposites doped with phosphoric acid still retained sufficient mechanical properties for use as proton exchange membranes.

3.5. Methanol permeability of PBI/silica nanocomposite membranes

Fig. 11 shows the methanol permeability of PBI10OH/silica nanocomposites and PBI30OH/silica nanocomposites. The methanol permeability of PBI10OH/silica nanocomposites and PBI30OH/silica nanocomposites decreased with increasing amounts of silica up to a silica content of 10 wt.%. It indicated that the methanol permeability of the nanocomposites decreased due to the silica particles acting as methanol barriers in the polymer matrix. The methanol permeability of PBI10OH/10 wt.% silica nanocomposites and PBI30OH/10 wt.% silica nanocomposites decreased 39 and 58% relative to the pure PBI10OH and PBI30OH copolymers, respectively. The larger decrease in methanol permeability of PBI30OH/10 wt.% silica nanocomposites could be attributed to more hydroxyl groups in the PBI30OH acting as bonding sites to the silica phase. However, a further increase in silica loading to 15 wt.% did not have any additional decrease in methanol permeability. This might be caused by a few agglomerated nanosized silica particles in the polymer matrix. Fig. 12 shows the methanol permeability of PBI10OH/silica nanocomposites and PBI30OH/silica nanocomposites doped with phosphoric acid. Compared to Fig. 11, it was found that the methanol permeability of the nanocomposites increased when they were doped with phosphoric acid. The increase in the methanol crossover in the acid-doped PBI/silica hybrid membranes could be due to the increase in the free volume of PBI after phosphoric acid doping because the protonation of PBI molecules could reduce the intermolecular interaction forces. Even though the permeability of the acid-doped PBI/silica hybrid membranes increased, it was still much lower than that of the Nafion® 117 membrane. We have used the same method to measure the permeability of the Nafion® 117 membrane, and found that it was 30×10^{-8} cm^2/s, as described in our previous paper [40].

3.6. Conductivity of PBI/silica nanocomposite membranes

Fig. 13 shows the proton conductivities of PBI30OH/silica nanocomposite membranes doped with different amounts of phosphoric acid. The measurement was taken at 160 °C under anhydrous condition, because the conductivity of the acid-doped PBI decreased above 160 °C due to the dehydration of the phosphoric acid, which turned into $H_4P_2O_7$. Compared with that of the acid-doped PBI membranes, the conductivity of the Nafion® 117 membrane declined abruptly above 80 °C, because of dehydration. The conductivity of the Nafion® 117 membrane could not be measured at 160 °C, because it lost proton conductive ability above 100 °C. The above-mentioned detail was discussed in our previous research [40]. The conductivities of the acid-doped PBI30OH/silica nanocomposite membranes increased with the doping level of phosphoric acid. However, the conductivities of the nanocomposite films were slightly lower than that of the

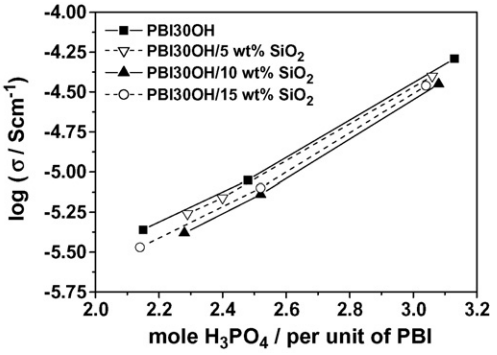

Fig. 13. Proton conductivity (σ) of PBI30OH/silica nanocomposite membranes doped with different amounts of phosphoric acid at 160 °C under anhydrous condition.

acid-doped pure PBI30OH membranes, because the silica particles in the polymer matrix might retard the mobility of protons in the membranes. It decreased by 22–28% with respect to the acid-doped pure PBI30OH membranes.

4. Conclusions

PBI/silica nanocomposite membranes can be prepared via sol–gel process from a fluorine-containing PBI copolymer with TEOS and a bonding agent due to the solubility of the fluorine-containing PBI copolymer. The introduction of the bonding agent results in the reinforcing interfacial interaction between PBI chains and the silica nanoparticles. The addition of silica can enhance the mechanical properties of the PBI membranes, and reduce the methanol permeability. Although the conductivity is slightly decreased by the silica, the overall performance of the nanocomposite membranes is still obviously improved by the addition of silica. The PBI/silica nanocomposite membranes have the potential for use as proton exchange membranes in high-temperature PEMFC.

Acknowledgements

The financial support provided by the National Science Council (Taiwan, ROC) through project NSC95-2221-E-006-186 is greatly appreciated. The authors also thank the Center for Micro/Nano Technology Research, National Cheng Kung University, Tainan, Taiwan, for equipment access and technical support.

References

[1] G. Inzelt, M. Pineri, J.W. Schultze, M.A. Vorotyntsev, Electron and proton conducting polymers: recent developments and prospects, Electrochim. Acta 45 (2000) 2403.
[2] M. Rikukawa, K. Sanui, Proton-conducting polymer electrolyte membranes based on hydrocarbon polymers, Prog. Polym. Sci. 25 (2000) 1463.
[3] L. Jorisen, V. Gogel, J. Kerres, J. Garche, New membranes for direct methanol fuel cells, J. Power Sources 105 (2002) 267.
[4] D.H. Jung, S.Y. Cho, D.H. Peck, D.R. Shin, J.S. Kim, Preparation and performance of a Nafion®/montmorillonite nanocomposite membrane for direct methanol fuel cell, J. Power Sources 118 (2003) 205.
[5] J.T. Wang, J.S. Wainright, R.F. Savinell, M. Litt, A direct methanol fuel cell using acid-doped polybenzimidazole as polymer electrolyte, J. Appl. Electrochem. 26 (1996) 751.
[6] Z.G. Shao, P. Joghee, I.M. Hsing, Preparation and characterization of hybrid Nafion–silica membrane doped with phosphotungstic acid for high temperature operation of proton exchange membrane fuel cells, J. Membr. Sci. 229 (2004) 43.
[7] V.V. Binsu, R.K. Nagarale, V.K. Shahi, Phosphonic acid functionalized aminopropyl triethoxysilane–PVA composite material: organic–inorganic hybrid proton-exchange membranes in aqueous media, J. Mater. Chem. 15 (2005) 4823.
[8] P. Staiti, M. Minutoli, Influence of composition and acid treatment on proton conduction of composite polybenzimidazole membranes, J. Power Sources 94 (2001) 9.
[9] J.S. Wainright, J.T. Wang, D. Weng, R.F. Savinell, M. Litt, Acid-dpoed polybenzimidazoles: a new polymer electrolyte, J. Electrochem. Soc. 142 (1995) L121.
[10] D.J. Jones, J. Roziere, Recent advances in the functionalisation of polybenzimidazole and polyetherketone for fuel cell applications, J. Membr. Sci. 185 (2001) 41.
[11] J.A. Asensio, S. Borros, P. Gomez-Romero, Proton-conducting polymers based on benzimidazoles and sulfonated benzimidazoles, J. Polym. Sci. Part A: Polym. Chem. 40 (2002) 3703.
[12] L. Xiao, H. Zhang, T. Jana, E. Scanlon, R. Chen, E.W. Choe, L.S. Ramanathan, S. Yu, B.C. Benicewicz, Synthesis and characterization of pyridine-based polybenzimidazoles for high temperature polymer electrolyte membrane fuel cell applications, Fuel Cells 5 (2005) 287.
[13] H.J. Kim, S.J. An, J.Y. Kim, J.K. Moon, S.Y. Cho, Y.C. Eun, H.K. Yoon, Y. Park, H.J. Kweon, E.M. Shin, Polybenzimidazoles for high temperature fuel cell applications, Macromol. Rapid Commun. 25 (2004) 1410.
[14] A. Schechter, R.F. Savinell, Imidazole and 1-methyl imidazole in phosphoric acid doped polybenzimidazole, electrolyte for fuel cells, Solid State Ionics 147 (2002) 181.
[15] M. Kawahara, J. Morita, M. Rikukawa, K. Sanui, N. Ogata, Synthesis and proton conductivity of thermally stable polymer electrolyte: poly(benzimidazole) complexes with strong acid molecules, Electrochim. Acta 45 (2000) 1395.
[16] J.M. Bae, I. Honma, M. Murata, T. Yamamoto, M. Rikukawa, N. Ogata, Properties of selected sulfonated polymers as proton-conducting electrolytes for polymer electrolyte fuel cells, Solid State Ionics 147 (2002) 189.
[17] H.L. Tyan, Y.C. Liu, K.H. Wei, Thermally and mechanically enhance clay/polyimide nanocomposite via reactive organoclay, Chem. Mater. 11 (1999) 1942.
[18] M.O. Abdalla, D. Dean, S. Campbell, Viscoelastic and mechanical properties of thermoset PMR-type polyimide–clay nanocomposites, Polymer 43 (2002) 5887.
[19] J. Zhang, B.K. Zhu, H.J. Chu, Y.Y. Xu, Silica/polyimide hybrids and their dielectric properties. I. Preparation with an improved sol–gel process with poly(amic acid) as the precursor, J. Appl. Polym. Sci. 97 (2005) 20.
[20] Z. Ahmad, J.E. Mark, Polyimide–ceramic hybrid composites by the sol–gel route, Chem. Mater. 13 (2001) 3320.
[21] R.K. Nagarale, G.S. Gohil, V.K. Shahi, R. Rangarajan, Organic–inorganic hybrid membrane: thermally stable cation-exchange membrane prepared by the sol–gel method, Macromolecules 37 (2004) 10023.
[22] M. Aparicio, Y. Castro, A. Duran, Synthesis and characterisation of proton conducting styrene-*co*-methacrylate–silica sol–gel membranes containing tungstophosphoric acid, Solid State Ionics 176 (2005) 333.
[23] O. Nishikawa, T. Sugimoto, S. Nomura, K. Doyama, K. Miyatake, H. Uchida, M. Watanabe, Preparation of the electrode for high temperature PEFCs using novel polymer electrolytes based on organic/inorganic nanohybrids, Electrochim. Acta 50 (2004) 667.
[24] C.N. Li, G.Q. Sun, S.Z. Ren, J. Liu, Q. Wang, Z.M. Wu, H. Sun, W. Jin, Casting Nafion-sulfonated organosilica nano-composite membranes used in direct methanol fuel cells, J. Membr. Sci. 272 (2006) 50.
[25] D.S. Kim, B.J. Liu, M.D. Guiver, Influence of silica content in sulfonated poly(arylene ether ether ketone ketone) (SPAEEKK) hybrid membranes on properties for fuel cell application, Polymer 47 (2006) 7871.
[26] R.C. Jiang, H.R. Kunz, J.M. Fenton, Composite silica/Nafion® membranes prepared by tetraethylorthosilicate sol–gel reaction and solution casting for direct methanol fuel cells, J. Membr. Sci. 272 (2006) 116.
[27] J. Premachandra, C. Kumudinie, W. Zhao, J.E. Mark, T.D. Dang, J.P. Chen, F.E. Arnold, Polymer–silica hybrid materials prepared from some functionalized polybenzoxazoles and polybenzobisthiazoles, J. Sol-Gel Sci. Technol. 7 (1996) 163.
[28] W.J. Lin, W.C. Chen, Synthesis and characterization of polyimide/oligomeric methylsilsesquioxane hybrid films, Polym. Int. 53 (2004) 1245.
[29] B.K. Chen, T.M. Chiu, S.Y. Tsay, Synthesis and characterization of polyimide/silica hybrid nanocomposites, J. Appl. Polym. Sci. 94 (2004) 382.
[30] V. Tricoli, Proton and methanol transport in poly(perfluorosulfonate) membranes containing Cs^+ and H^+ cations, J. Electrochem. Soc. 145 (1998) 3798.

[31] H.Y. Chang, C.W. Lin, Proton conducting membranes based on PEG/SiO_2 nanocomposites for direct methanol fuel cells, J. Membr. Sci. 218 (2003) 295.
[32] J.P. Chen, F.E. Arnold, Synthesis of functionalized high temperature benzoxazole polymers–silica hybrid materials, Polym. Mater. Sci. Eng. Proc. ACS Div. Polym. Mater. Sci. Eng. 70 (1993) 301.
[33] A.R. Kulkarni, Engineer polymer electrolytes with enhanced ionic conduction, Solid State Ionics 136 (2000) 549.
[34] M. Suzuki, T. Yoshida, T. Koyama, S. Kobayashi, M. Kimura, K. Hanabusa, H. Shirai, Ionic conduction in partially phosphorylated poly(vinyl alcohol) as polymer electrolytes, Polymer 41 (2000) 4531.
[35] Z.H. Huang, K.Y. Qiu, The effects of interactions on the properties of acrylic polymers/silica hybrid materials prepared by the in situ sol–gel process, Polymer 38 (1997) 521.
[36] Y. Wei, D.L. Jin, C.C. Yang, G. Wei, A fast convenient method to prepare hybrid sol–gel materials with low volume-shrinkages, J. Sol–Gel Sci. Technol. 7 (1996) 191.
[37] P. Musto, M. Abbate, M. Lavorgna, G. Ragosta, G. Scarinzi, Microstructural features, diffusion and molecular relaxations in polyimide/silica hybrids, Polymer 47 (2006) 6172.
[38] L.H. Wang, Y. Tian, H.Y. Ding, J.D. Li, Microstructure and properties of organosoluble polyimide/silica hybrid films, Eur. Polym. J. 42 (2006) 2921.
[39] J.J. Lin, X.D. Wang, Novel low-*k* polyimide/mesoporous silica composite films: preparation, microstructure, and properties, Polymer 48 (2007) 318.
[40] S-.W. Chuang, S.L-.C. Hsu, Synthesis and properties of a new fluorine-containing polybenzimidazole for high-temperature fuel-cell applications, J. Polym. Sci. Part A: Polym. Chem. 44 (2006) 4508.